Effect of Flow Rate on the Performance of an Evacuated Tilting Pad Journal Bearing: Load on Pad vs. Load-Between-Pad Configurations

Luis San Andrés[1(✉)] and Andy Alcantar[2]

[1] J. Mike Walker '66 Department of Mechanical Engineering, Texas A&M University College Station, Houston, TX 77843, USA
lsanandres@tamu.edu

[2] Bearing Group Miba Industrial Bearings U.S. (Houston) LLC, Houston, TX 77536, USA
andy.alcantar@miba.com

Abstract. Reducing the oil flow supplied to a fluid film bearing decreases the drag power loss and increases efficiency, though with increased pad temperatures and a drop in damping. Savings in pumping and lubricant storage make the case for low flow. The paper reports further measurements of performance in a tilting pad journal bearing with evacuated ends and configured as load on pad (LOP) and load between pads (LBP). The supplied flow (Q) ranges from 150% to 25% of a nominal flow rate (Q_s). Operation is at a constant shaft speed of 6 krpm and with unit loads as large as 2.07 MPa. Both bearings operate slightly more eccentrically as $Q < Q_s$, the LBP bearing displacing more. Pad temperatures are similar for both bearings, although the LOP bearing runs cooler and its oil exit temperature is also lower as Q decreases. The bearings main stiffness (K_{yy}) increases with load, the LOP bearing producing 25% more stiffness that increases as Q decreases. The LOP bearing produces small K_{xx} that quickly decreases for $Q = 25\%\ Q_s$. The LBP bearing does produce significant $K_{xx} \sim K_{yy}$, both slightly affected by flow reduction. The main damping C_{yy} for the LBP bearing drops quickly for the lowest Q, whereas C_{yy} for the LOP bearing remains unchanged. Similarly, C_{xx} for the LBP bearing varies little with Q decreasing, while for the LBP bearing, $C_{xx} \to 0$ for the lowest Q. The measurements show the LBP bearing performs better at low flows whereas the LOP bearing losses both stiffness and damping for the lowest Q. At this low flow, the bearing produced low frequency shaft motions (SSV Hash).

Keywords: Tilting Pad Bearing · Rotordynamic Force Coefficients · Stability

1 Introduction

Modern operation of tilting pad journal bearings (TPJBs) demands of reduced flow rates while keeping the pad temperatures within an acceptable limit for the Babbitt material (<130 °C) [1]. A reduced flow produces lesser drag power losses and increases the efficiency of the machinery [2], albeit reliability for long-term operation remains

F. Chu and Z. Qin (Eds.): IFToMM 2023, MMS 139, pp. 78–92, 2024.
https://doi.org/10.1007/978-3-031-40455-9_8

questionable. Other advantages include smaller pumping equipment and storage tanks. However, operation with a too low flow rate can produce subsynchronous shaft vibrations (SSV Hash) [3].

A concerted experimental research program at the Turbomachinery Laboratory aimed to quantify the effects of reduced flow rate on the performance of TPJBs, see Refs. [4–10]. The cited references present extensive critical reviews of the past literature, including modeling approaches and comparisons to experimental data. For the experiments, five and four-pad bearings are configured with ends seals for a flooded type, or without end seals to make them evacuated ends. The applied loads can be along the center of a pad or between pads, LOP and LBP respectively.

The tests include operation at two shaft speeds = 6 krpm and 12 krpm (= 64 m/s surface speed) and the applied unit loads range from 345 kPa to 2.07 MPa. The nominal flow rate (Q_s) is a function of the rotor surface speed, the number of pads and the pads' axial length, and the operating bearing clearance. In a typical test campaign, the supplied oil flow (Q) ranges from 1.5 Q_s to ¼ Q_s, and measurements included the bearing eccentricity (e) and attitude angle, the temperature rise downstream of the pads, loaded and unloaded, the oil exit temperature when leaving a bearing, the drag power losses from torque recordings, and the identification of force coefficients from dynamic loads applied and having a large frequency content.

In brief, as $Q < Q_s$, the experimental results show a moderate reduction in drag power losses accompanied by pad subsurface temperature rises. Too low Q's and large applied loads do produce too hot pad temperatures that approach the safe limit for Babbitt material. In general, the TPJBs direct stiffnesses ($K_{yy} > K_{xx}$) and damping ($C_{yy} \sim C_{xx}$) coefficients increase with both unit load (along Y) and shaft speed. Reduced flow rates $Q \rightarrow$ ½ Q_s do not significantly affect the bearings force coefficients. However, for very low flow rates, $Q \sim$ ¼ Q_s and lesser, there is a precipitous loss in both stiffness and damping coefficients. The LOP bearing performs the worst since both K_{xx} and $C_{xx} \rightarrow 0$ as $Q << Q_s$. SSV Hash emerged for extreme starved flow conditions and low loads.

Please refer to the References cited [4–8][1] and students theses [9, 10] for more details on the experimental campaigns, the major results and a thorough discussion of the findings. This paper reports further measurements of performance in a four-pads TPJB with evacuated ends, and configured as load on pad (LOP) and load between pads (LBP). The measurements complement those in Ref. [8] and compare the performance of a LOP bearing vs. that of a LBP bearing as the supplied flow rate varies from 1.5 Q_s to ¼ Q_s.

2 Description of Test Rig and Bearings

Figure 1 portrays the test rig used for the force evaluation, static and dynamic, of hydrodynamic fluid film bearings. Earlier references [4–8] fully describe the test rig, its major components and ancillary systems. A 40kW air turbine drives a solid rigid rotor supported on high-precision rolling element bearings housed in massive steel pedestals. A

[1] References [5] and [6] received best paper awards by the Structures and Dynamics Committee of the ASME International Gas Turbine Institute in 2022 and 2023, respectively.

split-parts bearing stator carries the test bearing, both installed in the middle section between the supporting rolling element bearings.

An external system supplies ISO VG 46 oil to the test bearing at a constant inlet temperature $T_{in} = 60$ °C, and a turbine type flow meter measures the lubricant volumetric supplied Q. Long rods (pitch stabilizers) with very low stiffness, hold the bearing stator assembly which includes ports for oil exit, as well as instrumentation for measurement of accelerations and displacements relative to the rotor along two orthogonal directions (X, Y).

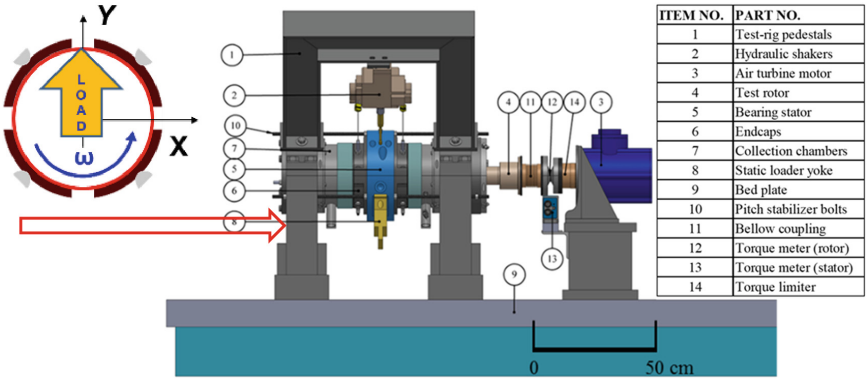

ITEM NO.	PART NO.
1	Test-rig pedestals
2	Hydraulic shakers
3	Air turbine motor
4	Test rotor
5	Bearing stator
6	Endcaps
7	Collection chambers
8	Static loader yoke
9	Bed plate
10	Pitch stabilizer bolts
11	Bellow coupling
12	Torque meter (rotor)
13	Torque meter (stator)
14	Torque limiter

Fig. 1. Side view of test rig and list of major components.

Figure 2 depicts the evacuated ends TPJB with oil supplied through spray bars. Individual separate arcuate plates retain each of the Babbitted pads constructed from AISI 1018 steel. The shaft diameter $D = 101.77$ mm and the bearing has four pads, each with axial length $L = 67$ mm and thickness $t = 19$ mm, and weighing 635 g. A pad is 72° in arc length and rests on a spherical pivot located at 50% pad offset. Table 1 lists other important bearing geometry and materials.

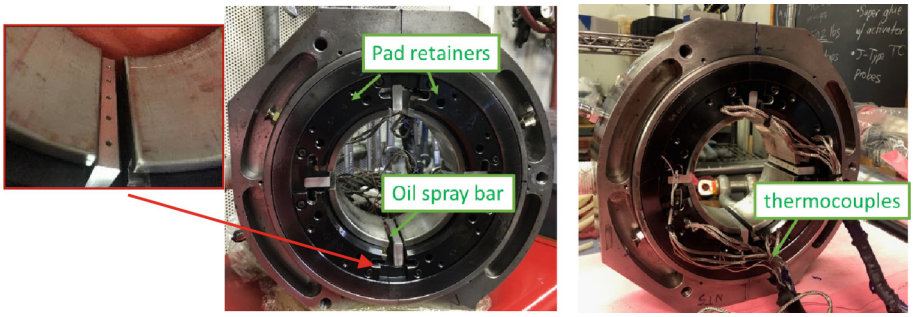

Fig. 2. Photographs of front and back sides of test bearing with evacuated ends.

Table 1. Four pad TPJB geometry and materials, Ref. [8]

Pad Clearance	$C_p = 134\ \mu\text{m} = C_r\ (1 + r)$
Pad Preload, r	$r = 0.30$
Bearing Room T clearance	$C_{rc} = 115\ \mu\text{m}$ measured
— Hot (After Test at 6 krpm)	$C_{rh} = 106\ \mu\text{m}$ measured
Spray bar (5 mm from pad edge)	Five orifices, diameter = 5/64 inch
Lubricant	ISO VG 46
Supply Temperature, T_s	60 °C
Viscosity (μ) at T_s	16.43 cPoise
Density (ρ) at T_s	838 kg/m^3
Specific heat (c_P)	2.08 kJ/(kg °C)
Viscosity-temperature Coefficient	0.0369 1/°C

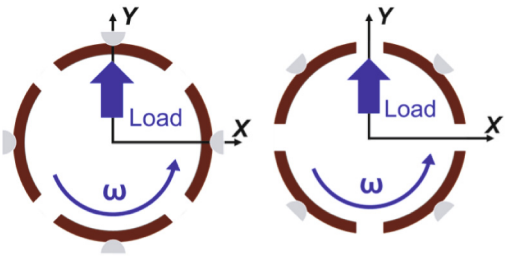

(a) LOP bearing (b) LBP bearing

Fig. 3. Schematic views of load on pad (LOP) and load between pads (LBP) bearings.

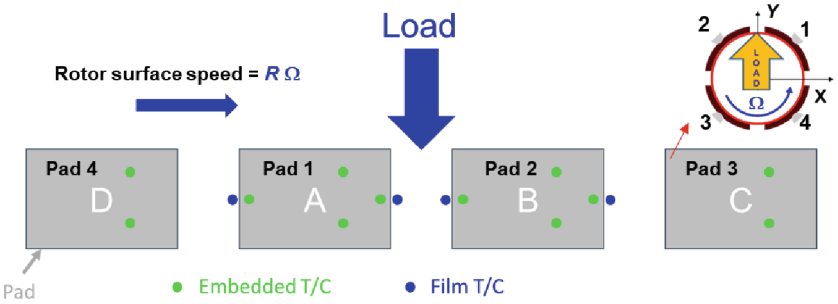

Fig. 4. Schematic depiction of thermocouples location for the LBP bearing.

3 Experimental Procedure

The experiments aim to quantify the performance of the test bearings, LOP and LBP, to significant variations in the supplied lubricant (Q), from 150% of a nominal condition to 25% (or less). In the tests, the rotor angular speed $\Omega = 6$ krpm and the applied load ranged from 2.13 kN to 12.8 kN. The specific load ($W/(LD)$) ranged from 0.345 MPa to 2.07 MPa for the LBP bearing, and 0.345 MPa to 1.38 MPa for the LOP bearing.

At 6 krpm, the rotor surface speed $U = ½\ D\ \Omega = 32$ m/s, and the nominal flow rate (Q_s) is proportional to the number of pads, ½ U, the pad axial length L, the bearing clearance C_r, and an empirical factor ($\lambda < 1$) that denotes the fraction of the flow leaving a pad trailing edge that enters the downstream pad at its leading edge. That is, Q_s is the flow that must fully wet (fill in) the bearing clearance at a no-load condition ($W = 0$). Presently, as determined from prior tests in Ref. [10], $Q_s = 14.4$ L per minute (LPM). Do realize the nominal supplied flow is only a function of shaft speed and operating clearance, and has no direct relation to the lubricant viscosity.

Prior art [11] details the dynamic load measurement procedure along with the identification process carried in the frequency domain. The bearing and its stator are represented as a lumped mass (M_{BC}) that displaces along two degrees of freedom (X,Y), as shown in Fig. 3. The stator elastic supports and the test bearing produce reactions to external forces applied by the shakers. The dynamic forces encompass an ensemble of loads with pseudo-random amplitude and frequencies, typically spaced 10 Hz. First, one shaker excites the test bearing with load $\mathbf{F_X} = [f_x = \sum f_k\ e^{i\omega kt}, f_y = 0]^{\mathrm{T}}$ that produces dynamic motion $\mathbf{z_X} = [x_x, y_x]^{\mathrm{T}}$ and acceleration $\mathbf{a_X} = [a_{xx}, a_{yx}]^{\mathrm{T}}$. Note that $\mathbf{z_X}$ is the relative displacement between the rotor and the bearing, and $\mathbf{a_X}$ is the absolute acceleration of the bearing stator. Next, the other shaker exerts the excitation $\mathbf{F_Y} = [f_x = 0, f_y = \sum f_k\ e^{i\omega kt}]^{\mathrm{T}}$ to produce the displacement $\mathbf{z_Y} = [x_y, y_y]^{\mathrm{T}}$ and acceleration $\mathbf{a_Y} = [a_{xy}, a_{yy}]^{\mathrm{T}}$. Sensors and a data acquisition system record the applied forces and ensuing motions, displacement and acceleration, of the bearing stator along the X and Y directions.

Next, a Discrete Fourier Transformation (DFT) transfers the recorded time domain data into the frequency domain, i.e., $\mathbf{F}_{\mathbf{X}(\omega)} = \mathrm{DFT}(\mathbf{F}_{\mathbf{X}(t)})$. The procedure calls for forming the (2x2) matrices of external forces $\mathbf{F}_{(\omega)} = [\mathbf{F}_{\mathbf{X}(\omega)} \mid \mathbf{F}_{\mathbf{Y}(\omega)}]$, bearing stator acceleration $\mathbf{a}_{(\omega)} = [\mathbf{a}_{\mathbf{X}(\omega)} \mid \mathbf{a}_{\mathbf{Y}(\omega)}]$ and displacements $\mathbf{z}_{(\omega)} = [\mathbf{z}_{\mathbf{X}(\omega)} \mid \mathbf{z}_{\mathbf{Y}(\omega)}]$. The test system has a complex dynamic stiffness matrix ($\mathbf{H}$) determined from.[2]

$$\mathbf{H}_{(\omega)} = [\mathbf{F} - M_{BC}\mathbf{a}]_{(\omega)}\mathbf{z}^{-1} \tag{1}$$

where $\mathbf{H} = [\ H_{xx}\ H_{xy} \mid H_{yx}\ H_{yy}]$ is the matrix of complex dynamic stiffnesses, and whose real and imaginary parts are curve fitted with stiffness, damping and virtual mass coefficients $(K, C, M)_{\alpha,\beta=x,y}$.

$$\mathrm{Re}\big(\mathbf{H}_{(\omega)}\big) \rightarrow \mathbf{K} - \omega^2\mathbf{M},\ \mathrm{Im}\big(\mathbf{H}_{(\omega)}\big) \rightarrow i\omega\mathbf{C} \tag{2}$$

[2] For simplicity in the discussion, Eq. (1) omits the (small) forces from the elastic rods holding the bearing stator.

In general for a TPJB, the cross-coupled force coefficients are much smaller than the direct force coefficients, i.e., $|H_{xy}|$ and $|H_{yx}| < < |H_{xx}|$ or $|H_{yy}|$, except for $Q < < Q_s$. For more details see Ref. [10].

4 Experimental Results and Discussion

4.1 Bearing Eccentricity

Figure 5 depicts the bearing eccentricity (e) for increasing specific loads and with flow rates ranging from 1.5 Q_s to 0.2 Q_s (=3.4 LPM) for the LBP bearing, and from 1.5 Q_s to 0.35 Q_s (=5 LPM) for the LOP bearing. In Fig. 5b, the graphs include dashed vertical lines denoting the nominal flow (Q_s = 14.4 LPM) at the operating speed of 6 krpm. Compared to the LBP bearing, the LOP bearing operates with a smaller eccentricity (e) that is not affected as the flow rate drops to 50% nominal. On the other hand, the LBP bearing shows a sharp increase in e for the smallest load (345 kPa) as Q drops to 20% of nominal.

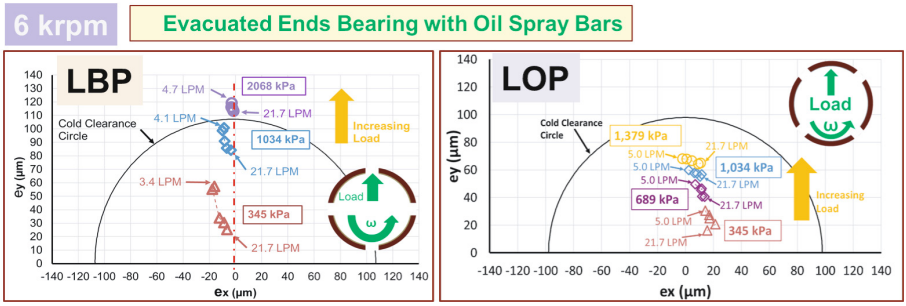

(a) e_y vs. e_x

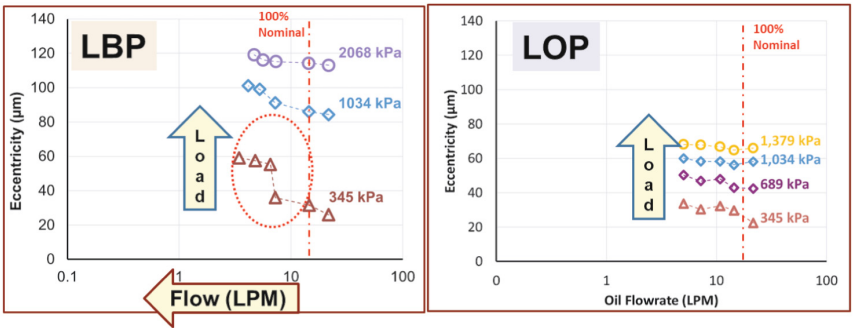

(b) e vs. Q. Load increases

Fig. 5. (a) Locus of bearing center (e_y vs. e_x) for increasing loads and a range of flow rates Q, (b) Bearing eccentricity (e) vs. flow rate (Q) for a range of specific loads ($W/(LD)$).

Note that the bearing eccentricity shown is relative to the hot center identified without any imposed load. Recall, the applied static load on the bearing is along the Y-direction

for both LOP or LBP configurations. Thus, as shown in Fig. 5b, the LOP bearing center (e) displaces nearly parallel to the load direction, i.e., $e_x < < e_y$. The LBP bearing, on the other hand, shows a sizeable displacement (e_x) orthogonal to the applied load W along Y. For the highest specific load of 2.07 MPa, the LBP bearing displaces to an eccentricity (e) that exceeds the cold clearance ($C_{rc} = 0.115$ mm). This behavior is not unusual as found in past measurements conducted with the LBP bearing configured with end seals (flooded condition); see Refs. [5, 6].

4.2 Pad Temperatures and Oil Exit Temperature

Figure 6 depicts the pad sub-surface temperature rise $\Delta T = (T\text{-}T_s)$ vs. flow rate for increasing specific loads. Figure 6a shows the largest temperature rise in the loaded pads. Note the specific loads and smallest flow rates (Q) are distinct for the LOP and LBP bearing cases; hence, a direct comparison of results is not immediately apparent, except for the smallest unit loads of 345 kPa and 1,034 kPa. For the 100% nominal flow (Q_s), both bearings produce the same temperature rise that increases as the unit load increases. In general, as Q reduces to 20% Q_s for the LBP bearing and 35% Q_s for the LOP bearing, ΔT rises by at most 10 °C and 5 °C respectively.

Figure 6b shows the largest temperature rise in the unloaded pads. For both bearings, LOP and LBP, ΔT is not a function of the applied load and slowly increases as Q decreases ($< Q_s$). At the lowest flow, ΔT is at most 10 °C higher than the temperature rise recorded for the nominal (100%) flow.

Note that the largest ΔT at the loaded pads does not reach the Babbitt recommended safe limit of 130 °C (70 °C above $T_s = 60$ °C). More temperature measurements reported in Refs. [5–7] do show temperature rises reaching the operational limit for very low flow rates and under high loads.

Figure 7 presents the measured oil exit temperature rise $\Delta T_E = (T_E\text{-}T_s)$ vs. flow and various unit loads. For the LOP bearing, independent of the applied load, the oil exit temperature rises by at most 5 °C as the supplied flow (Q) drops to 35% Q_s. On the other hand, for the LBP bearing, ΔT_E increases by at most 15 °C as $Q = 0.25\ Q_s$ and the largest applied load of 2.07 MPa. The photograph in the inset depicts a thermographic image of the bearing housing. Note the red color denotes the highest temperatures that occur on the bearing caps located on the sides of the test bearing. The caps collect the exit oil and a drain holes route the hot lubricant to the return sump and heat exchanger. Incidentally, the recorded oil exit temperatures are not representative of the temperatures in the bearing pads (shown in Figs. 6).

Typically, the shear induced drag power loss (P_{loss}) in a fluid film bearing is estimated from the product of the flow rate (Q) and the oil exit temperature rise ΔT_E. That is, $P_{loss} \sim (c_P\ \rho\ Q\ \Delta T_E)$, not shown here for brevity. See Refs. [4, 5] for complete details including the measurement of the drag torque that directly leads to P_{loss}. However, one can readily infer from the supplied Q and the measured ΔT_E that P_{loss} decreases by at most 25% for the lowest Q and a unit load of 1.034 MPa. The savings in P_{loss} are not too significant at the operating speed of 6 krpm. Not so for operation at 12 krpm, as shown in Ref. [8]. In the same reference, P_{loss} for the evacuated bearing is significantly lower than that for the flooded bearing.

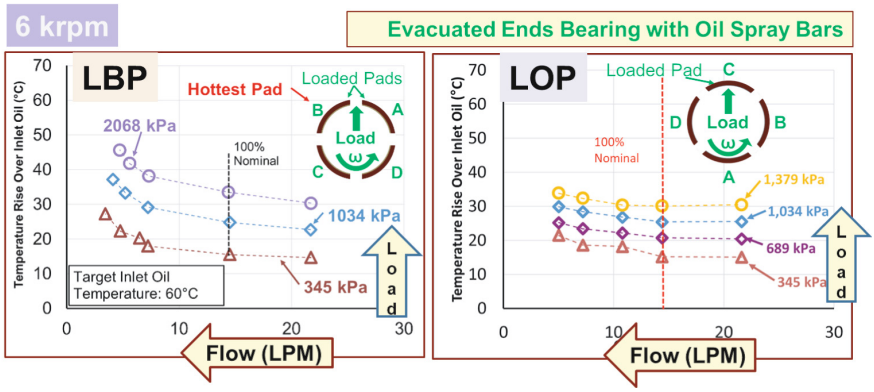

(a) Peak temperature rise in loaded pads of evacuated ends TPJB

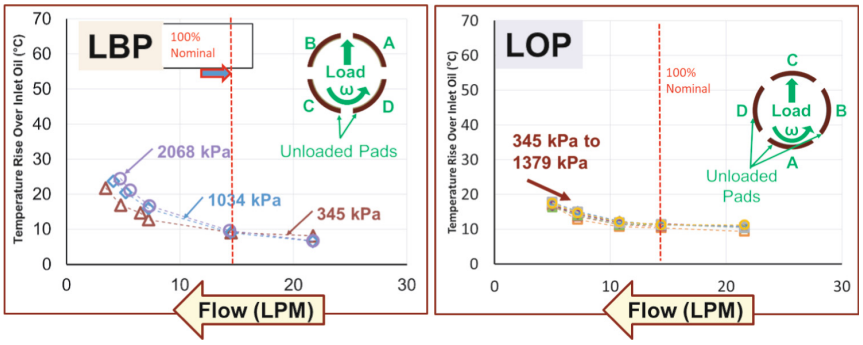

(b) Peak temperature rise in unloaded pads of test bearing

Fig. 6. (a) Loaded pads largest temperature rise and (b) unloaded pads temperature rise vs. flow rate (Q) over a range of specific loads ($W/(LD)$). Temperature rise relative to oil inlet temperature $T_s = 60$ °C.

4.3 Force Coefficients for LOP and LBP Bearings with Evacuated Ends

Figure 8 presents samples of the experimentally obtained LOP bearing complex stiffnesses, real and imaginary parts, vs. frequency under two applied loads and two flow rates, 35% and 150% of Q_s. For the bearing type, $\mathrm{Re}(H_{yy}) > \mathrm{Re}(H_{xx})$ and $\mathrm{Im}(H_{yy}) > \mathrm{Im}(H_{xx})$, in particular for the moderate unit load of 1,379 kPa. Note the cross coupled coefficients H_{yx} and H_{xy} have the same order of magnitude as H_{xx}. In general, the direct complex stiffnesses significantly increase as the applied load increases and as the flow rate (Q) decreases. The $\mathrm{Im}(H)$'s are proportional to the excitation frequency, hence the bearing provides constant damping coefficients since $\mathrm{Im}(H_{xx}) \rightarrow (\omega\, C_{xx})$,for example. It is important to realize that $\mathrm{Im}(H_{xx})$ for a 35% Q_s is much smaller than the one for the 150% nominal flow.

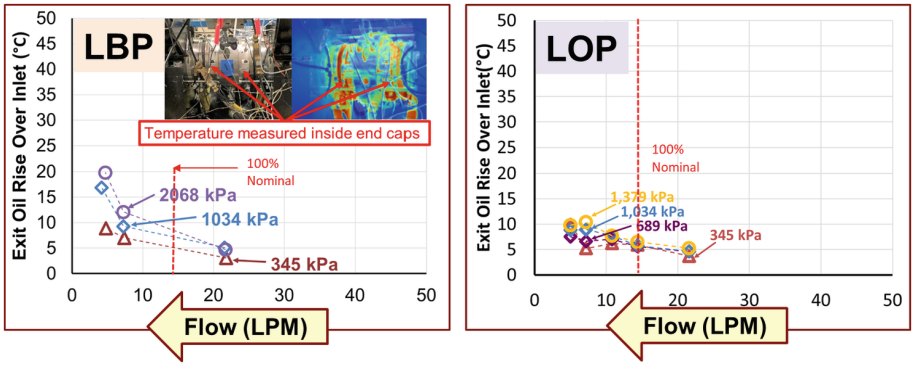

Fig. 7. Oil exit temperature rise vs. flow rate (Q) over a range of specific loads ($W/(LD)$). Temperature rise relative to oil inlet temperature $T_s = 60$ °C.

Figures 9 and 10 depict the direct stiffnesses (K_{yy}, K_{xx}) and damping coefficients (C_{yy}, C_{xx}) estimated from the complex stiffnesses (**H**) vs. the supplied flow. Recall that for both the LBP and LOP bearings the Y direction coincides with the applied load (W). From the results in Fig. 9, for the LOP bearing notice that the (load) stiffness $K_{yy} >> K_{xx}$, whereas $K_{yy} \sim K_{xx}$ for the LPB bearing. For both bearings, K_{yy} substantially increases as the applied load increases. Importantly enough, K_{yy} slightly grows as the flow rate decreases below the nominal condition ($Q < Q_s$), an expected outcome since the film thickness decreases as the flow reduces. The most surprising outcome relates to the LOP bearing stiffness K_{xx} (orthogonal to W direction) that is not a function of the applied load and quickly decreases as the flow reduces. In fact, $K_{xx} \to 0$ for the smallest Q, which means the lateral pads could become statically unstable.

The curve fits $\text{Re}(H) \to (K\text{-}\omega^2 M)$ deliver virtual mass coefficients (M) with significant magnitudes. The said coefficients are not shown for brevity; see Refs. [7, 8] for example. Presently, the LOP bearing gives $M_{yy} \sim 35$ kg and slightly increasing with load; hence $\text{Re}(H_{yy})$ softens with frequency, as seen in Fig. 8. Similarly, $M_{xx} \sim 40$ kg and quickly decreases as Q drops. On the other hand, the LBP bearing has $M_{yy} \sim$ - 20 kg and which decreases further as Q falls below Q_s. Hence, $\text{Re}(H_{yy})$ hardens with frequency. In the same fashion, $M_{xx} \sim$ -10 kg at Q_s and begins to increase for the lowest $Q = 0.25\ Q_s$.

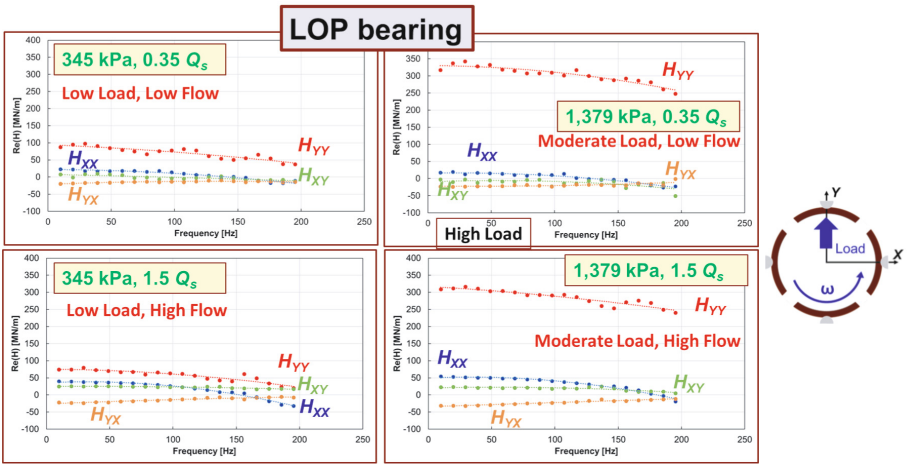

(a) Real part of LOP bearing complex stiffnesses (**H**)

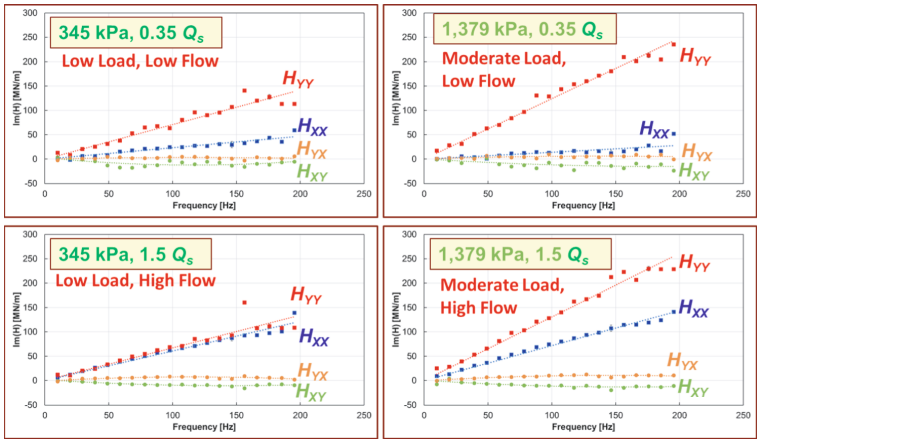

(b) Imaginary part of LOP bearing complex stiffnesses (**H**)

Fig. 8. Real and imaginary parts of complex stiffness (**H**) vs. excitation frequency. Results for LOP bearing: unit loads ($W/(LD)$) = 345 kPa (left graphs) and 1,379 kPa (right graphs) and two flow rates $Q = 35\%\ Q_s$ (top graphs) and $150\%\ Q_s$ (bottom graphs). Operation at 6 krpm (surface speed = 32 m/s).

Similarly, shown in Fig. 10, the direct damping coefficients (C_{yy}, C_{xx}) for the LBP bearing are similar in magnitude and C_{yy} decreases as Q drops. The applied load does increase C_{yy} but not as strongly as the direct stiffness K_{yy} does. The LBP bearing, on the other hand, shows $C_{yy} > C_{xx}$, and with the coefficient C_{yy} not affected by a reduction on the supplied flow below the nominal condition. As with the coefficient K_{xx}, the damping

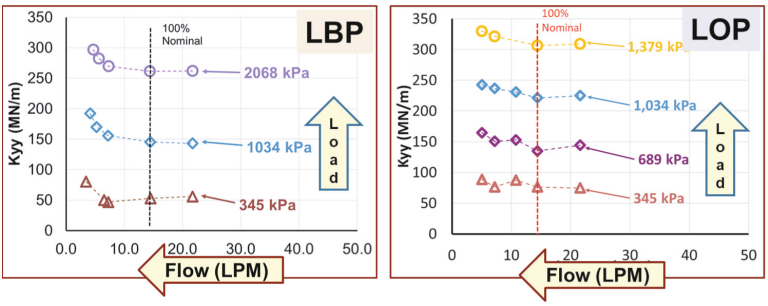

(a) Stiffness K_{yy} vs. Q

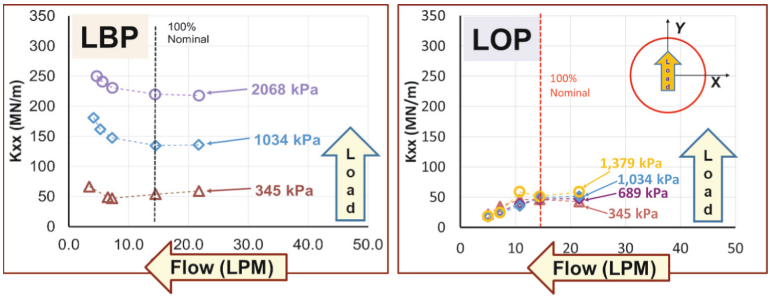

(b) Stiffness K_{xx} vs. Q

Fig. 9. Direct stiffnesses K_{yy} and K_{xx} (top and bottom graphs) vs. flow rate (Q) and various specific loads ($W/(LD)$). Results for LBP bearing (left graphs) and LOP bearing (right graphs). Operation at 6 krpm (surface speed = 32 m/s). Y is the direction of applied static load (W).

coefficient C_{xx} shows a precipitous drop as soon as the flow rate falls below nominal, $Q < Q_s$. The sudden reduction in damping is independent of the applied load and evidences the unloaded pads (along X direction) severely starve of lubricant. Clearly, since K_{xx} and $C_{xx} \rightarrow 0$, then the bearing would be both statically and dynamically unstable, and which would certainly induce SSV Hash at very low frequencies. Ref. [8] provides details on the amplitude and frequency content of the bearing SSV motions.

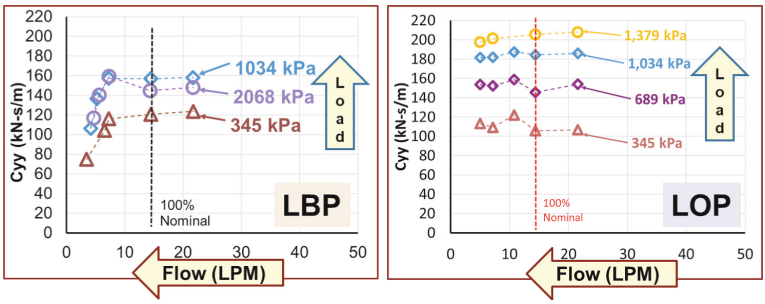

(a) Damping C_{yy} vs. Q

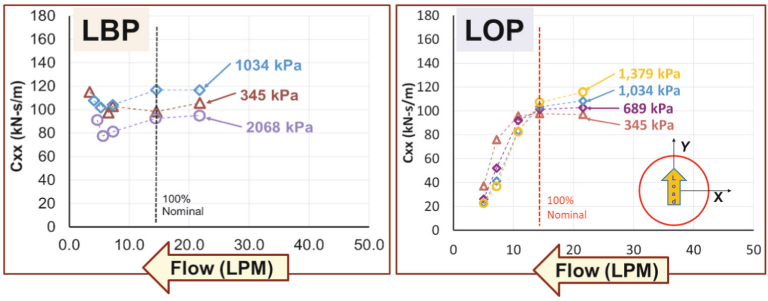

(b) Damping C_{xx} vs. Q

Fig. 10. Direct damping C_{yy} and C_{xx} (top and bottom graphs) vs. flow rate (Q) and various specific loads ($W/(LD)$). Results for LBP bearing (left graphs) and LOP bearing (right graphs). Operation at 6 krpm (surface speed = 32 m/s).

5 Conclusion

The paper presented measurements of performance for a four-pad tilting pad journal bearing with evacuated ends. The bearing is configured as load on pad (LOP) and load between pads (LBP). Operation is at a constant shaft speed of 6 krpm (surface speed = 32 m/s) and with unit loads as large as 2.07 MPa. In the tests, the supplied flow (Q) of an ISO VG oil delivered at 60 °C ranges from 150% to 25% of a nominal 100% rate Q_s = 14.4 L per minute. The major findings of the experimental campaign are:

- A reduction in Q ($< Q_s$) makes both bearings operate slightly more off-center, the LBP bearing displaces more.
- Pad subsurface temperatures are similar for both bearings, although the LOP bearing is colder by a few Celsius degrees, and its oil exit temperature is also lower as the flow decreases well below nominal.
- The bearings direct stiffness K_{yy} along the load direction (Y) increases with load, the LOP bearing producing 25% more stiffness and which increases as Q decreases. The LOP bearing produces a smaller stiffness K_{xx}, that quickly drops to reach nearly zero as Q drops to 25% Q_s. The LBP bearing does produce significant stiffness K_{xx} (~ K_{yy}), and both stiffnesses increase as Q reduces.

- The LBP bearing shows a negative virtual mass coefficient M_{yy}, hence the bearing dynamic stiffness hardens with excitation frequency. In opposition, the LOP bearing produces $M_{yy} > 0$, and the bearing softens as the excitation frequency increases.
- The direct damping coefficient C_{yy} for the LBP bearing drops quickly for the lowest Q, whereas C_{yy} for the LOP bearing remains impervious to flow changes. Similarly, C_{xx} varies little with a flow reduction.
- On the other hand, C_{xx} for the LOP bearing dramatically drops toward null for the lowest flow rate, Q =0.25 Q_s.
- Hence, the LBP bearing is more tolerant to significant flow reductions than the LOP bearing is. For the lowest Q, this last bearing type entirely lost its stiffness and damping coefficients in a direction orthogonal to the applied load. Under this extreme operating condition, the LOP bearing produced low frequency subsynchronous shaft motions (SSV Hash).

Lastly, under no circumstances the test bearings operated for extended periods of time with a too low flow rate that could have degraded the lubricant and bearing pads' Babbitted surfaces.

Acknowledgment. The authors acknowledge the financial support of the Turbomachinery Research Consortium and the personal research funds of Dr. L. San Andrés. Thanks to undergraduate student Mr. Zihan Ouyang for assisting to operate and maintain the test rig.

Abbreviations

NOMENCLATURE

C_r	Bearing radial clearance [m]
$C_{\alpha\beta}$	Bearing damping coefficients, $\alpha, \beta = x,y$ [Ns/m]
c_P	Lubricant specific heat [J/(kg ^{o}C)]
D	Shaft diameter [m]
e	Bearing eccentricity [m]
$H_{\alpha\beta}$	Bearing complex dynamic stiffnesses, $\alpha, \beta = x,y$ [N/m]
$K_{\alpha\beta}$	Bearing static stiffness coefficients, $\alpha, \beta = x,y$ [N/m]
L	Bearing length [m]
$M_{\alpha\beta}$	Bearing virtual mass coefficients, $\alpha, \beta = x,y$ [N/m]
M_{BC}	Bearing housing and assembly mass [kg]
P_{loss}	~ $c_P\ \rho\ Q\ \Delta\ T_E$. Estimated drag power loss [W]
Q	Supplied flow rate [m^3/s], Q_s nominal flow rate [m^3/s]
T	Temperature [^{o}C]
T_s, T_E	Oil inlet and exit temperatures [^{o}C]
X,Y	Coordinate system
W	Applied static load (along Y) [N]
$\Delta\ T$	(T-T_s). Temperature difference [^{o}C]
ρ, μ	Oil density [kg/m^3] and viscosity [Pa.s]
Ω	Rotor angular speed [rad/s]
ω	Excitation frequency [rad/s

Vectors and matrices

a $[a_x, a_y]^{\mathbf{T}}$**.** Vector of bearing acceleration [m/s^2]
F $[F_x, F_y]^{\mathbf{T}}$**.** Vector of applied forces [N]
H $[H_{xx}, H_{xy} \mid H_{yx}, H_{yy}]$**.** Matrix of complex dynamic stiffnesses [N/m]
z $[x, y]^{\mathbf{T}}$**.** Vector of bearing displacements relative to shaft [m]

Abbreviations

LBP Load between pads
LOP Load on pad
LPM Liters per minute
SSV Subsynchronous vibration
TBJB Tilting pad journal bearing

References

1. Leopard, A.J.: Tilting pad bearings-limits of operation. ASLE Lubrication Eng. **32**(2), 637–644 (1976)
2. Dmochowski, W.M., Blair, B.: Effect of oil evacuation on the static and dynamic properties of tilting pad journal bearings. Trib. Trans. 49 (2006)
3. DeCamillo, S., He, M., Cloud, C.H., Byrne, J.: Journal bearing vibration and SSV hash. In: Proceedings of the 37th Turbomachinery Symposium, The Turbomachinery Laboratory, Texas A&M University, September 7–11, Houston, TX, USA, pp. 179–194 (2008). https://doi.org/10.21423/R1DH1J
4. San Andrés, L., Jani, H., Kaizar, H., Thorat, M.: On the effect of supplied flow rate to the performance of a tilting-pad journal bearing. - static load and dynamic force measurements. ASME J. Gas Turbines Power **142**(2), 121006 (2020). https://doi.org/10.1115/1.4048798
5. San Andrés, L., Toner, J., Alcantar, A.: Measurements to quantify the effect of a reduced flow rate on the performance of a tilting pad Journal Bearing (LBP) with flooded ends. ASME J. Eng. Gas Turbines Power **143**(11), 111012 (2021). ASME Paper GT2021–58771. https://doi.org/10.1115/1.4052268
6. San Andrés, L., Alcantar, A.J.: Effect of reduced oil flow rate on the static and dynamic performance of a tilting pad journal bearing running in both flooded and evacuated conditions. ASME J. Eng. Gas Turbines Power **145**(6), 061012 (2023). ASME Paper GT2022-81839. https://doi.org/10.1115/1.4056535
7. San Andrés, L., Alcantar, A.: Effect of reduced oil flow rate on the static and dynamic performance of a tilting pad journal bearing running in both the flooded and evacuated conditions. In: Proceedings of the 50th Turbomachinery & Pump Symposia, Houston, TX, December 2021
8. San Andrés, L., Ouyang, Z., Qin, Y.: Effect of reduced oil flow on the performance of a load on pad, tilting pad journal bearing: flooded vs. evacuated conditions. In: Proceedings of ASME Turbo Expo 2023, Turbomachinery Technical Conference and Exposition, Boston. ASME Paper GT2023-103242 (2023). https://hdl.handle.net/1969.1/196726
9. Jani, H.: Measurements of the Static and Dynamic Force Performance on a Five-Pad, Spherical-Pivot Tilting-Pad Journal Bearing: Influence of Oil Flow Rate. M.S. thesis, Texas A&M University, College Station, TX, USA (2018)

10. Toner, J.: Measurements of the Static and Dynamic Force Performance on a Five-Pad, Spherical-Pivot Tilting-Pad Journal Bearing: Influence of Oil Flow Rate. M.S. thesis, Texas A&M University, College Station, TX, USA (2020)
11. San Andrés, L.: Experimental identification of bearing force coefficients. Modern Lubrication Theory, Notes 14, Libraries Texas A&M University Repository (2009). http://oaktrust.library.tamu.edu/handle/1969.1/93197. Accessed Jan 2021